

# Proton emission off nuclei induced by kaons in flight

V. K. Magas<sup>1</sup>, J. Yamagata-Sekihara<sup>2,3</sup>, S. Hirenzaki<sup>4</sup>, E. Oset<sup>3</sup>,  
A. Ramos<sup>1</sup>

<sup>1</sup>*Departament d'Estructura i Constituents de la Matèria, Universitat de Barcelona,  
Diagonal 647, E-08028 Barcelona, Spain*

<sup>2</sup>*Yukawa Institute for Theoretical Physics, Kyoto University, Kyoto 606-8502, Japan*

<sup>3</sup>*Departamento de Física Teórica and IFIC, Centro Mixto Universidad de Valencia-CSIC,  
Institutos de Investigación de Paterna, Apartado 22085, 46071 Valencia, Spain*

<sup>4</sup>*Department of Physics, Nara Women's University, Nara 630-8506, Japan*

September 24, 2018

## Abstract

We study the  $(K^-, p)$  reaction on nuclei with a 1 GeV/c momentum kaon beam, paying a special attention at the region of emitted protons having kinetic energy above 600 MeV, which was used to claim a deeply attractive kaon nucleus optical potential. Our model describes the nuclear reaction in the framework of a local density approach and the calculations are performed following two different procedures: one is based on a many-body method using the Lindhard function and the other one is based on a Monte Carlo simulation. The simulation method offers flexibility to account for processes other than kaon quasi-elastic scattering, like  $K^-$  absorption by one and two nucleons producing hyperons, and allows to consider final state interactions of the  $K^-$ ,  $p$  and all other primary and secondary particles on their way out of the nucleus, as well as the weak decay of the produced hyperons into  $\pi N$ . We find a limited sensitivity of the cross section to the strength of the kaon optical potential. We also show serious drawback in the experimental set up from the requirement of having, together with the energetic proton, at least one charged particle detected in the decay counter surrounding the target, since we find that the shape of the original cross section is appreciably distorted, to the point of invalidating the claims made in the experimental paper on the strength of the kaon nucleus optical.

## 1 Introduction

The issue of the kaon interaction in the nucleus has attracted much attention in past years. Although from the study of kaonic atoms one knows that the  $K^-$ -nucleus potential

is attractive [1], the discussion centers on how attractive the potential is and if it can accommodate deeply bound kaonic atoms (kaonic nuclei), which could be observed in direct reactions. A sufficiently large attraction could even make possible the existence of kaon condensates in nuclei, which has been suggested in [2]. Stimulated by the success in reproducing the data of kaonic atoms, many works considered strongly attractive potentials of the order of 200 MeV at normal nuclear matter density [3–7], or explored the dependence of a few observables to a wide range of depths from 0 to 200 MeV [8–10]. More moderate attraction is found in similar works done in [11–13]. Yet, all modern potentials based on underlying chiral dynamics of the Kaon-nucleon interaction [14–18] lead to moderate potentials of the order of 60 MeV attraction at nuclear matter density. They also have a large imaginary part making the width of the deeply bound states much larger than the energy separation between the levels, which would rule out the experimental observation of peaks. The agreement with the data of kaonic atoms of this purely theoretical shallow potential is good [19], and a fit to all data adding a small phenomenological potential to the theoretical one performed in [20] indicates that the best fit potential deviates at most by 20% from the theoretical one of [15].

The opposite extreme is represented by some highly attractive phenomenological potentials with about 600 MeV strength in the center of the nucleus [21,22]. These potentials, leading to compressed nuclear matter of ten times nuclear matter density, met criticisms from [23] and more recently from [24], which were rebutted in [25] and followed by further argumentation in [26] and [27]. More recently the lightest K-nuclear system of  $\bar{K}NN$  has also been the subject of strong debate [28–31].

Experimentally, the great excitement generated by peaks seen at KEK [32] and FINUDA [33,34], originally interpreted in terms of deeply bound kaons atoms, is receding, particularly after the work of [23], regarding the KEK experiment, and those of [35–37], regarding the FINUDA ones, found explanations of the experimental peaks based on conventional reactions that unavoidably occur in the process of kaon absorption. Also the thoughts of [38], with opposite views to those of FINUDA in [34], and the reanalysis of the KEK proton spectrum from  $K^-$  absorption on  $^4\text{He}$  [32], done in [39], where the original narrow peak appears much broader and is consistent with the signal seen on a heavier  $^6\text{Li}$  target in FINUDA [40], have helped to bring the discussion to more realistic terms. Nevertheless, the possibility that the FINUDA peak of [33] could be a signal of a deeply bound kaon state is still defended [41]. This brief description just shows the intense activity and strong interest in this subject over the past few years.

There are also claims (with very low statistical significance) of  $K^-pp$  and  $K^-ppn$  bound states from  $\bar{p}$  annihilation in  $^4\text{He}$  at rest measured by OBELIX@CERN [42], as well as the recent claim of a  $K^-pp$  bound state, seen from the  $pp \rightarrow K^+X$  reaction by the DISTO experiment [43]. These experimental claims are under investigation now since, before calling in new physics, it is important to make clear that these data cannot be explained with conventional mechanisms.

In this work we focus on yet another experiment which led the authors to claim evidence for a very strong kaon-nucleons potential, with a depth of the order of 200 MeV [44]. The experiment looks for fast protons emitted from the absorption of in flight kaons by nuclei.

Our aim is to show how this experiment was analyzed and which ingredients are missing. Throughout this work we shall see that the interpretation of the data requires a more thorough analysis, and with all things considered, we reach different conclusions than those of Ref. [44], in the sense that we do not find evidence for a strongly attractive kaon-nucleus optical potential.

One of the shortcomings of Ref. [44] stems from employing the Green's function method [45] in a variant used in [46–48] to analyze the data and extract from there the kaon optical potential. The only mechanism considered in Ref. [44] for the emission of fast protons is the  $\bar{K}p \rightarrow \bar{K}p$  process, taking into account the optical potential for the slow kaon in the final state. However, there are other mechanisms that contribute to generate fast protons, namely kaon absorption by one nucleon,  $K^-N \rightarrow \pi\Sigma$  or  $K^-N \rightarrow \pi\Lambda$  followed by decay of the  $\Sigma$  or the  $\Lambda$  into  $\pi N$ , or the absorption by pairs of nucleons,  $\bar{K}NN \rightarrow \Sigma N$  and  $\bar{K}NN \rightarrow \Lambda N$ , followed also by similar hyperon decays. The contributions from these processes were also suggested in Ref. [49]. In the present work, we take into account these additional mechanisms by means of a Monte Carlo simulation, while the processes involving  $\bar{K}N$  scattering, which are dominant in this reaction, are considered in two different ways, one based on standard many body methods using Lindhard functions and another one based on a Monte Carlo simulation. The agreement of the two calculational methods gives us confidence to use the Monte Carlo simulation for the processes involving more than one step and/or one nucleon and two nucleon kaon absorption.

## 2 The $(K^-, p)$ reaction in nuclei: many body approach

We are dealing here with an inclusive reaction, where a kaon in flight hits a nucleus and a proton is emitted. In the present case we focus on fast protons, which could be emitted when the kaons are trapped in the nucleus or are rescattered with small energy. The reaction is inclusive in the sense that, apart from the proton observed, anything can happen to the nucleus. In fact many processes may take place. The original kaon can undergo quasi-elastic collisions with the nucleons, transferring them some energy. The kaon can be absorbed, either by one nucleon or by pairs of nucleons. The kaon can be trapped in a kaonic orbit, etc. Once a kaon has experienced a particular reaction, the final products also suffer their own interactions with the nucleus before, eventually, a fast proton gets out. Complicated as it may sound—and we shall deal with these complications in a following section—the evaluation of the inclusive cross section is however easy since one is looking for the most energetic protons and in the forward direction, which means that these protons must take the largest possible energy from the original kaon. In other words, if a kaon undergoes a quasi-elastic collision in which the proton does not fall in this narrow window, the event will be dismissed because this kaon, having lost a fraction of its energy, will not have a second chance of producing a fast proton again. Obviously, if the kaon is absorbed it disappears from the flux and must also be eliminated in the evaluation of further processes (the contribution from the absorption mechanisms will be calculated later). The other relevant observation is that if the final fast proton has a secondary collision it will also

loose energy and will not lie in the desired energy window. In practical terms this means that we can just care about the direct  $K^-p \rightarrow K^-p$  quasi-elastic reaction at a certain point in the nucleus and distort the initial  $K^-$  and final proton waves. These type of reactions have received much attention and we describe here the standard procedure of dealing with them [50, 51].

Diagrammatically, the process considered is depicted in Fig. 1, which shows the kaon inducing a  $ph$  excitation and remaining in the nucleus, representing what we call a quasi-elastic collision. The kaon transfers energy and momentum to a nucleon that is promoted from below to above the (local) Fermi sea.

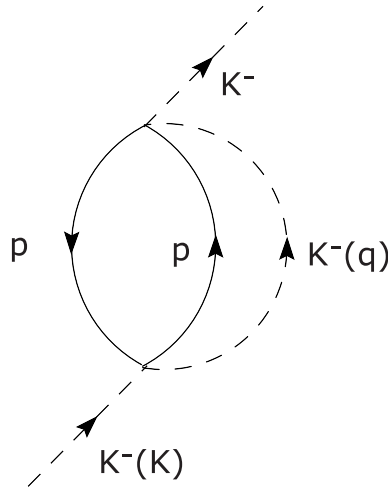


Figure 1: Diagrammatic representation of the inclusive  $(K^-, p)$  reaction.

The kaon self-energy for the diagram of Fig. 1 in a Fermi sea is given by

$$-i\Pi_{\text{qe}}(k) = \int \frac{d^4q}{(2\pi)^4} i\bar{U}(k-q)(-i)T(-i)T \frac{i}{q^{02} - \vec{q}^2 - m_K^2 - \Pi(q)}, \quad (1)$$

where  $\bar{U}(k-q)$  is the Lindhard function for  $ph$  excitation and  $T$  stands for the  $K^-p \rightarrow K^-p$  scattering matrix. The factor  $[q^{02} - \vec{q}^2 - m_K^2 - \Pi(q^0, \vec{q})]^{-1}$  is the kaon propagator which includes its self-energy in the medium,  $\Pi(q^0, \vec{q})$ . Using the Cutkosky rules one easily obtains the imaginary part of  $\Pi_{\text{qe}}(k)$  as in [52],

$$\Pi_{\text{qe}} \rightarrow 2i\text{Im} \Pi_{\text{qe}}, \quad (2)$$

$$\bar{U}(k-q) \rightarrow 2i\theta(k^0 - q^0)\text{Im} \bar{U}(k-q), \quad (3)$$

$$D(q) = \frac{1}{q^{02} - \vec{q}^2 - m_K^2 - \Pi(q)} \rightarrow 2i\theta(q^0)\text{Im} D(q). \quad (4)$$

Then

$$\text{Im} \Pi_{\text{qe}}(k) = -2 \int \frac{d^4q}{(2\pi)^4} \text{Im} \bar{U}(k-q) |T|^2 \text{Im} \frac{1}{q^{02} - \vec{q}^2 - m_K^2 - \Pi(q^0, \vec{q})}, \quad (5)$$

where  $\bar{U}$  is given by

$$\bar{U}(k - q) = 2 \int \frac{d^3 p_N}{(2\pi)^3} \frac{M}{E(\vec{p}_N)} \frac{M}{E(\vec{k} + \vec{p}_N - \vec{q})} \frac{n(\vec{p}_N)[1 - n(\vec{k} + \vec{p}_N - \vec{q})]}{k^0 + p_N^0 - q^0 - E_{N'}(\vec{k} + \vec{p}_N - \vec{q}) + i\epsilon}. \quad (6)$$

The fast protons with momentum  $\vec{k} + \vec{p}_N - \vec{q}$  are the energetic ones that would be observed, hence the corresponding Pauli blocking factor,  $1 - n$ , is just unity here. From Eq. (6) one obtains  $\text{Im } \bar{U}$  as

$$\text{Im } \bar{U} = -2\pi \int \frac{d^3 p_N}{(2\pi)^3} \frac{M}{E(\vec{p}_N)} \frac{M}{E(\vec{k} + \vec{p}_N - \vec{q})} n(\vec{p}_N) \delta(k^0 + E(\vec{p}_N) - q^0 - \Delta - E(\vec{k} + \vec{p}_N - \vec{q})), \quad (7)$$

where we have introduced an energy gap between the energy of the holes and the energy of the particles [53, 54]. We thus obtain for  $\text{Im } \Pi_{\text{qe}}$  the following equation

$$\begin{aligned} \text{Im } \Pi_{\text{qe}}(k) &= 2 \int \frac{d^3 p_N}{(2\pi)^3} n(\vec{p}_N) \frac{M}{E(\vec{p}_N)} \int \frac{d^3 q}{(2\pi)^3} |T|^2 \frac{M}{E(\vec{k} + \vec{p}_N - \vec{q})} \\ &\quad \times \text{Im} \frac{1}{q^0{}^2 - \vec{q}^2 - m_K^2 - \Pi(q^0, \vec{q})} \Big|_{q^0 = k^0 + E(\vec{p}_N) - \Delta - E(\vec{k} + \vec{p}_N - \vec{q})}. \end{aligned} \quad (8)$$

The physical interpretation comes by recalling that

$$2\omega V_{\text{opt}} \equiv \Pi_{\text{qe}}, \quad (9)$$

$$\text{Im } V_{\text{opt}} = \frac{1}{2\omega} \text{Im } \Pi_{\text{qe}}, \quad (10)$$

$$\Gamma = -2\text{Im } V_{\text{opt}} = -\frac{\text{Im } \Pi_{\text{qe}}}{\omega}, \quad (11)$$

where  $\omega$  is the kaon energy and  $V_{\text{opt}}$  is the  $K^-$ -nucleus optical potential. Our states are normalized to unity in a box of volume  $V$ . The flux of the incoming kaons is  $v_{K^-}/V$  and thus the  $K^-$  cross section with the nucleons of the Fermi sea of volume  $V$  is given by

$$\sigma = \frac{\Gamma}{K^- \text{ flux}} = \frac{\Gamma}{v_{K^-}/V} = V \frac{\Gamma}{k}. \quad (12)$$

Replacing  $V$  by an integral  $\int d^3 r$  over the nuclear density we obtain, upon the change of variables

$$\vec{p} \equiv \vec{k} + \vec{p}_N - \vec{q}, \quad (13)$$

where  $\vec{p}$  is the outgoing proton variable,

$$\begin{aligned} \sigma &= -\frac{2}{k} \int d^3 r \int \frac{d^3 p_N}{(2\pi)^3} n(\vec{p}_N, \vec{r}) \frac{M}{E(\vec{p}_N)} \\ &\quad \times \int \frac{d^3 p}{(2\pi)^3} |T|^2 \frac{M}{E(\vec{p})} \text{Im} \frac{1}{q^0{}^2 - \vec{q}^2 - m_K^2 - \Pi(q^0, \vec{q})} \Big|_{\substack{q^0 = k^0 + E(\vec{p}_N) - \Delta - E(\vec{p}) \\ \vec{q} = \vec{k} + \vec{p}_N - \vec{p}}}, \end{aligned} \quad (14)$$

from where

$$\begin{aligned} \frac{d\sigma}{d\Omega(\hat{p})E(\vec{p})} &= -\frac{2}{k}pM \int d^3r \int \frac{d^3p_N}{(2\pi)^3} n(\vec{p}_N, \vec{r}) \frac{M}{E(\vec{p}_N)} \\ &\times \frac{1}{(2\pi)^3} |T|^2 \text{Im} \frac{1}{q^0{}^2 - \vec{q}^2 - m_K^2 - \Pi(q^0, \vec{q})} \Big|_{\vec{q}=\vec{k}+\vec{p}_N-\vec{p}}^{q^0=k^0+E(\vec{p}_N)-\Delta-E(\vec{p})}. \end{aligned} \quad (15)$$

The integral over  $\vec{r}$  covers the size of the nucleus. As in previous works [35, 36], we use a realistic nuclear density profile for  $^{12}\text{C}$ , given by three-parameter Fermi distribution [55], which reproduces elastic electron scattering data. We have also tried a more sophisticated nuclear density profile, which accounts for the finite range of the interaction via a folding procedure, and is preferred by the antiprotonic X-rays and radiochemical data [56]. Although the folded density is almost 10% lower in the center of nuclei and extends to larger distances, the final result of our simulation is practically unaffected by this density change. The integral over  $\vec{p}_N$  is restricted to the hole (bound) nucleon states within the local Fermi momentum  $k_F(\vec{r})$  obtained from the nuclear density at point  $\vec{r}$ . This is accounted for by the Pauli blocking factor  $n(\vec{p}_N, \vec{r})$ .

In free space, the cross section for kaon scattering off a proton in the lab frame with the proton emerging in the forward direction reads

$$\left. \frac{d\sigma}{d\Omega(\hat{p})} \right|_{\text{lab}} = \frac{\pi}{k} \frac{1}{(2\pi)^3} \bar{p}^2 |T|^2 \frac{M}{2} \frac{1}{\bar{p}(k^0 + M) - E(\bar{p})k}, \quad (16)$$

where  $\bar{p}$  is the momentum of the nucleon

$$\bar{p} = \frac{2p_{\text{CM}}E_{\text{CM}}}{M}, \quad p_{\text{CM}} = \frac{\lambda^{1/2}(s, m_K^2, M^2)}{2\sqrt{s}}. \quad (17)$$

Equation (16) establishes a link between  $|T|^2$  and the forward cross section, which can be implemented into Eq. (15) to derive our final formula

$$\begin{aligned} \frac{d\sigma}{d\Omega(\hat{p})E(\vec{p})} &= -\frac{4p}{\bar{p}^2} \left. \frac{d\sigma}{d\Omega(\hat{p})} \right|_{\text{lab}} \int d^3r e^{-\int_{-\infty}^{\infty} \sigma_{\rho}(b, z') dz'} \int \frac{d^3p_N}{(2\pi)^3} n(\vec{p}_N, \vec{r}) \frac{M}{E(\vec{p}_N)} \theta(q^0) \\ &\times [\bar{p}(k^0 + M) - E(\bar{p})k] \frac{1}{\pi} \text{Im} \frac{1}{q^0{}^2 - \vec{q}^2 - m_K^2 - \Pi(q^0, \vec{q})} \Big|_{\vec{q}=\vec{k}+\vec{p}_N-\vec{p}}^{q^0=k^0+E(\vec{p}_N)-\Delta-E(\vec{p})}, \end{aligned} \quad (18)$$

where we have added the distortion factor for the initial  $K^-$  and the final proton  $p$  (exponential factor in the equation), as well as the factor  $\theta(q^0)$  of Eq. (4). Taking into account that  $\langle \sigma_{K^-N}^{\text{tot}} \rangle \simeq 45 \text{ mb} \simeq \langle \sigma_{pN} \rangle \equiv \sigma$  for  $K^-$ -nucleon collisions with  $p_{K^-} \simeq 1 \text{ GeV}/c$  and proton-nucleon collisions with protons having about 600–700 MeV kinetic energy, we have implemented a combined eikonal distortion factor as in [44, 46]

$$\int d^3r \rightarrow \int d^3r e^{-\int_{-\infty}^{\infty} \sigma_{\rho}(b, z') dz'}, \quad (19)$$

where  $b$  is the impact parameter  $b^2 = x^2 + y^2$ .

The backward differential cross section of the elementary process  $K^-p \rightarrow K^-p$  in the laboratory frame  $(d\sigma/d\Omega)_{\text{lab}}$  for incoming kaons of 1 GeV/c is taken to be 8.8 mb/sr, using the  $K^-p$  elastic cross-section data of Ref. [57]. We note that the authors of Ref. [17] take a value of 3.6 mb/sr as an effective way to implement effects of Fermi motion, Pauli blocking, etc, which here we consider explicitly.

### 3 Monte Carlo simulation

The procedure outlined above is quite efficient to produce the cross section for the  $(K^-, p)$  reaction, but obviously including only the quasi-elastic collisions  $K^-p \rightarrow K^-p$ . There might be other processes contributing to generate fast protons and, when this is the case, it becomes advisable to make a simulation of the reaction. This procedure has been developed in Ref. [58] for the study of inclusive pionic reactions in nuclei and has also been applied to other processes, such as photon induced pion and proton emission in nuclei [52, 59], electron induced proton emission [60], nucleon emission following hypernuclear decay [61, 62], nucleon emission following kaon absorption in nuclei [35], etc.

As sources of fast protons we consider the quasi-elastic  $K^-N$  scattering process, as well as the absorption of the kaon by one and two nucleons. The election of which reaction occurs at a certain point in the nucleus is done as usual. One chooses a step size  $\delta l$  and calculates, by means of  $\sigma_i \rho \delta l$  with  $i = \text{qe}, 1\text{N}, 2\text{N}$ , the probabilities that any of the possible reactions happens. The values of the cross sections are discussed in Sect. 4. The size of  $\delta l$  is small enough such that the sum of probabilities that any reaction occurs is reasonably smaller than unity. A random number from 0 to 1 is generated and a reaction occurs if the number falls within the corresponding segment of length given by its probability, the segments being put successively in the interval [0-1]. If the random number falls outside the sum of all segments then this means that no reaction has been taken place and the kaon is allowed to proceed one further step  $\delta l$ .

#### 3.1 Quasi-elastic scattering

We here describe how the Monte Carlo simulation treats the quasi-elastic reaction discussed in Sect. 2. The general strategy is to let the kaon propagate through the nucleus determining, at each step  $\delta l$ , whether it can undergo a quasi-elastic collision, according to the probability  $\sigma_{\text{qe}} \rho \delta l$ , where  $\sigma_{\text{qe}}$  is the  $K^-N \rightarrow K^-N$  elastic cross section. If there is a quasi-elastic collision at a certain point, then the initial  $K^-$  momentum and the nucleon momentum, randomly chosen within the Fermi sea, are boosted to their CM frame. The direction of the scattered momenta is determined according to the experimental cross section. A boost to the lab frame determines the final kaon and nucleon momenta. The event is kept as long as the size of the nucleon momentum is larger than the local value of  $k_F$ . Since we take into account secondary collisions we consider the reactions  $K^-p \rightarrow K^-p$ ,  $K^-p \rightarrow K^0n$  and  $K^-n \rightarrow K^-n$  with their corresponding cross sections.

Once primary nucleons are produced they are also followed through the nucleus taking into account the probability that they collide with other nucleons, losing energy and changing their direction. We follow the procedure detailed in [58,59].

We also follow the rescattered kaon on its way through the nucleus. In the subsequent interaction process we let the kaon experience whichever reaction of the three that we consider (quasi-elastic, one body absorption, two body absorption) according to their probabilities. If the kaon remains after the collision, this procedure continues until it finally emerges out of the nucleus or it is absorbed by one or two nucleons.

### 3.2 One body kaon absorption

We consider the reactions  $K^-N \rightarrow \pi\Lambda$  and  $K^-N \rightarrow \pi\Sigma$ , with all the possible charge combinations. Once again the probability of this occurring is weighed by their corresponding cross sections and the directions of the  $\pi$  and of the hyperons are also determined in the CM frame. The system is then boosted back to the lab frame, where we let the  $\Lambda$  or the  $\Sigma$  propagate through the nucleus, undergoing quasi-elastic collisions with the nucleons. Once they leave the nucleus they are allowed to decay weakly into  $\pi N$  providing in this way a source of protons which is not negligible, as we will see.

### 3.3 Two body absorption

We also take into account the following processes:  $K^-NN \rightarrow \Lambda N$  or  $K^-NN \rightarrow \Sigma N$  with all possible charge combinations. The probability per unit length for two nucleon absorption,  $\mu_{K^-NN}$ , together with the distribution into the different possible channels, are discussed in Sect. 4. In these reactions an energetic nucleon is produced, as well as a  $\Lambda$  or a  $\Sigma$  hyperon. Both the nucleon and the hyperon are followed through the nucleus as discussed above. Once out of the nucleus, the hyperon is let to decay weakly into  $\pi N$  pairs. Therefore, the two body absorption process provides a double source of fast protons, those directly produced in the absorption reactions and those coming from hyperon decays.

### 3.4 Consideration of the $K^-$ optical potential

We also take into account a kaon optical potential  $V_{\text{opt}} = \text{Re} V_{\text{opt}} + i \text{Im} V_{\text{opt}}$ , which will influence the kaon propagation through the nucleus, especially after a high momentum transfer quasi-elastic collision when the kaon will acquire a relatively low momentum.

As discussed in the introduction, one can find in the literature quite different values for the real part of the potential. In the present study we vary the strength of the potential,  $\text{Re} V_{\text{opt}}$ , to study the sensitivity of the results: starting from  $-60 \rho/\rho_0$  [14–18], going through  $-200 \rho/\rho_0$  MeV [3–10], and down to  $-600 \rho/\rho_0$  MeV [21, 22]. For the imaginary part of the optical potential we take  $\text{Im} V_{\text{opt}} \approx -60 \rho/\rho_0$  MeV, as in the experimental paper [44] and the theoretical study of [15].

In the presence of an optical potential, the kaon spectral function has the form:

$$S_K(\tilde{M}_K) = \frac{1}{\pi} \frac{-2M_K \text{Im} V_{\text{opt}}}{(\tilde{M}_K^2 - M_K^2 - 2M_K \text{Re} V_{\text{opt}})^2 + (2M_K \text{Im} V_{\text{opt}})^2}. \quad (20)$$

In the Monte Carlo simulation we implement this distribution by generating a random kaon mass  $\tilde{M}_K$  around a central value,  $M_K + \text{Re} V_{\text{opt}}$ , which is the bare kaon mass shifted by the real part of the optical potential. The generated random masses lie within a certain extension determined by the width of the distribution  $\Gamma_K = -2\text{Im} V_{\text{opt}}$ , the size of which is controlled by the imaginary part of the optical potential. The probability assigned to each value of  $\tilde{M}_K$  follows the Breit-Wigner distribution given by the kaon spectral function.

### 3.5 Final observable

After all the processes implemented in the Monte Carlo simulation, some particles leave the nucleus, and we select the events that contain a fast proton in the region of interest. To adapt the calculations to the experiment of [44] we keep the protons that emerge within an angle of 4.1 degrees in the nuclear rest frame (lab frame). For quasi-elastic scattering processes this would correspond to events in which the kaons emerge backwards in the  $\bar{K}N$  CM frame and the protons are most energetic, having of the order of 500 – 700 MeV of kinetic energy in the lab frame.

To facilitate comparison with experiment, the missing invariant mass of the  $^{12}\text{C}(K^-, p)$  reaction is converted into a binding energy of the kaon,  $E_B$ , should the process correspond to the trapping of a kaon in a bound state and emission of the fast proton, according to

$$\sqrt{(E_K + M_{^{12}\text{C}} - E_p)^2 - (\vec{P}_p - \vec{P}_K)^2} = M_{^{11}\text{B}} + M_K - E_B, \quad (21)$$

where  $E_p, \vec{P}_p$  are the energy and momentum of the observed proton and  $E_K, \vec{P}_K$  are the energy and momentum of the initial kaon.

### 3.6 Coincidence simulation

It is very important to keep in mind that the measurements in the experiment of [44] were done in coincidence. The outgoing proton was measured by the KURAMA spectrometer in the forward direction, while another detector, the decay counter, was sandwiching the target. The published spectra was obtained with a requirement of having an outgoing proton in the KURAMA spectrometer and at least one charged particle in the decay counter [63].

Obviously, the real simulation of such a coincidence experiment is tremendously difficult, practically impossible with high accuracy, because it would require tracing all the charged particles coming out from all possible scatterings and decays. Although we are studying many processes and following many particles in our Monte Carlo simulation, which is not the case in the Green function method used in the data analysis [44], we can not simulate precisely the real coincidence effect.

What we can do is to eliminate the processes which, for sure, will not produce a coincidence, a procedure that we refer to as minimal coincidence requirement [68]. If the kaon in the first quasi-elastic scattering produces an energetic proton falling into the peaked region of the spectra, then the emerging kaon will be scattered backwards. In our Monte Carlo simulation we can select events where neither the proton nor the kaon will have any further reaction after such a scattering. In these cases, although there is a “good” outgoing proton, there are no charged particles emerging with the right direction with respect to the beam axis to hit a decay counter, since the  $K^-$  escapes undetected through the backward direction. Therefore, this type of events must be eliminated for comparison with the experimental spectra.

As we will see in the next section, the main source of the energetic protons is  $K^-p$  quasi-elastic scattering and, therefore, the minimal coincidence requirement removes a substantial part of the potentially “good” events changing the form of the final spectrum. Furthermore, events with one or two nucleon absorption or/and with several quasi-elastic rescatterings have a good chance of producing a charged particle that goes through the decay counter. Thus, the final spectrum obtained from our Monte Carlo simulations with minimal coincidence requirement will probably overshoot the experimental spectrum by an amount which will depend on the capability of the events having the given energy  $E_B$  of producing, apart from the corresponding energetic proton, additional charged particles hitting the decay counters.

## 4 Input cross sections

### 4.1 $\bar{K}N$ cross sections

The elastic and inelastic two body  $\bar{K}N$  cross sections for kaons of about 1 GeV/c are taken from the Particle Data Group (PDG) [64]. The values are the following:

$$\sigma_{K^-p \rightarrow K^-p} = 21.22 \text{ mb}, \quad \sigma_{K^-p \rightarrow \bar{K}^0n} = 7.15 \text{ mb}, \quad \sigma_{K^-n \rightarrow K^-n} = 18.5 \text{ mb}$$

$$\sigma_{K^-p \rightarrow \pi^0\Lambda} = 4.32 \text{ mb}, \quad \sigma_{K^-p \rightarrow \pi^+\Sigma^-} = 1.76 \text{ mb}$$

$$\sigma_{K^-p \rightarrow \pi^-\Sigma^+} = 1.4 \text{ mb}, \quad \sigma_{K^-p \rightarrow \pi^0\Sigma^0} = 1.58 \text{ mb}$$

$$\sigma_{K^-n \rightarrow \pi^-\Lambda} = 6.35 \text{ mb}, \quad \sigma_{K^-n \rightarrow \pi^-\Sigma^0} = 0.97 \text{ mb}, \quad \sigma_{K^-n \rightarrow \pi^0\Sigma^-} = 1.15 \text{ mb}$$

From the PDG we also know the total cross-sections:

$$\sigma_{K^-p}^{\text{tot}} = 51.7 \text{ mb}, \quad \sigma_{K^-n}^{\text{tot}} = 38 \text{ mb} \quad \Rightarrow \quad \langle \sigma_{K^-N}^{\text{tot}} \rangle = 45 \text{ mb} \quad [\text{see Eq. (18)}].$$

Since these are larger than the sum of the partial cross sections that we are using explicitly, we define:

$$\sigma_{K^-p \rightarrow X} = 14.27 \text{ mb}, \quad \sigma_{K^-n \rightarrow X} = 10.0 \text{ mb},$$

which take care about all possible reaction channels, like  $K^-p \rightarrow \eta\Lambda$ ,  $K^-p \rightarrow \eta\Sigma$  and others, where no fast nucleons come out. Thus, we introduce an extra segment of length

$\sigma_{K^-p,n \rightarrow X} \rho \delta l$  in the interval [0-1] for the Monte Carlo decision of these reactions to occur. If this is the case, the  $K^-$  simply disappears, since the particles produced in these reactions can not contribute to our observable.

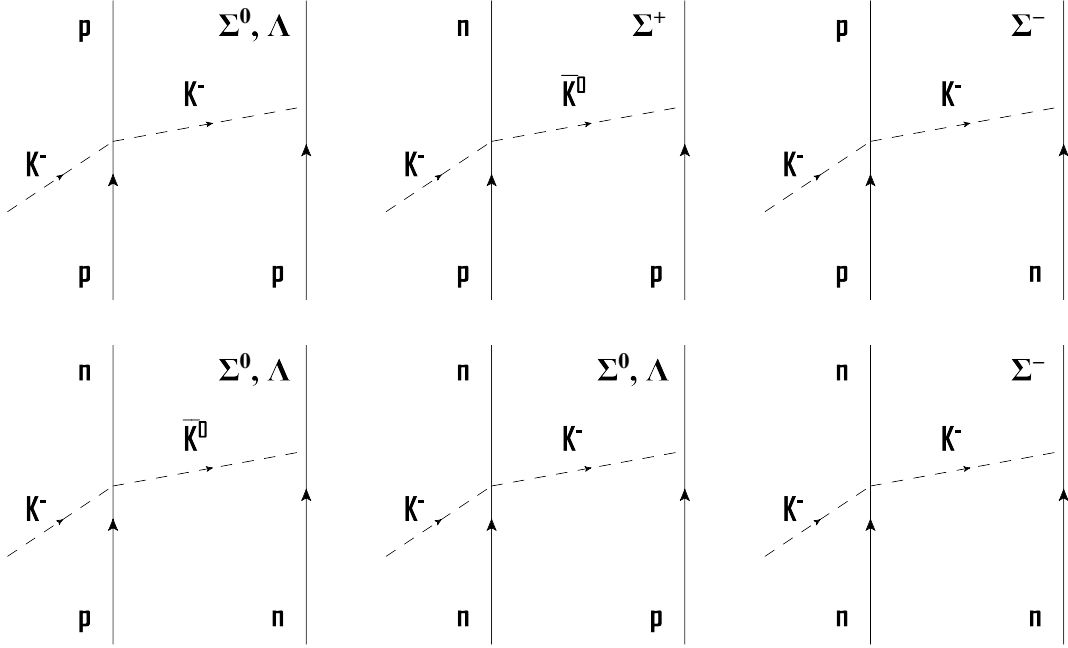


Figure 2: The two nucleon  $K^-$  absorption diagrams from a kaon-exchange picture.

## 4.2 Two nucleon absorption cross-sections

The probability per unit length for two nucleon absorption is proportional to the square of the nucleon density:

$$\mu_{K^-NN}(\rho) = C_{\text{abs}}\rho^2.$$

We assume a total two body absorption rate of 20% that of one body absorption at about nuclear matter density, something that one can infer from data of  $K^-$  absorption in  $^4\text{He}$  [65]. In practice, this is implemented in the following way:

$$\langle \mu_{K^-NN} \rangle = C_{\text{abs}} \langle \rho^2 \rangle = 0.2 \langle \mu_{K^-N} \rangle = 0.2 \langle \sigma_{K^-N}^{\text{tot}} \rangle \langle \rho \rangle,$$

where  $\sigma_{K^-N}^{\text{tot}}$  accounts for the total one nucleon absorption cross section and, in symmetric nuclear matter, it is given by:

$$\langle \sigma_{K^-N}^{\text{tot}} \rangle = (\sigma_{K^-p}^{\text{tot}} + \sigma_{K^-n}^{\text{tot}} - \sigma_{K^-p \rightarrow K^-p} - \sigma_{K^-n \rightarrow K^-n})/2 = 21.45 \text{ mb}.$$

Taking  $\langle \rho \rangle = \rho_0/2$ , where  $\rho_0 = 0.17 \text{ fm}^{-3}$  is normal nuclear matter density, we obtain

$$C_{\text{abs}} \approx 6 \text{ fm}^5.$$

The different partial processes that can take place in a two nucleon absorption reaction are:

$$K^- pp \rightarrow p\Lambda, p\Sigma^0, n\Sigma^+$$

$$K^- pn \rightarrow n\Lambda, n\Sigma^0, p\Sigma^-$$

$$K^- nn \rightarrow n\Sigma^- .$$

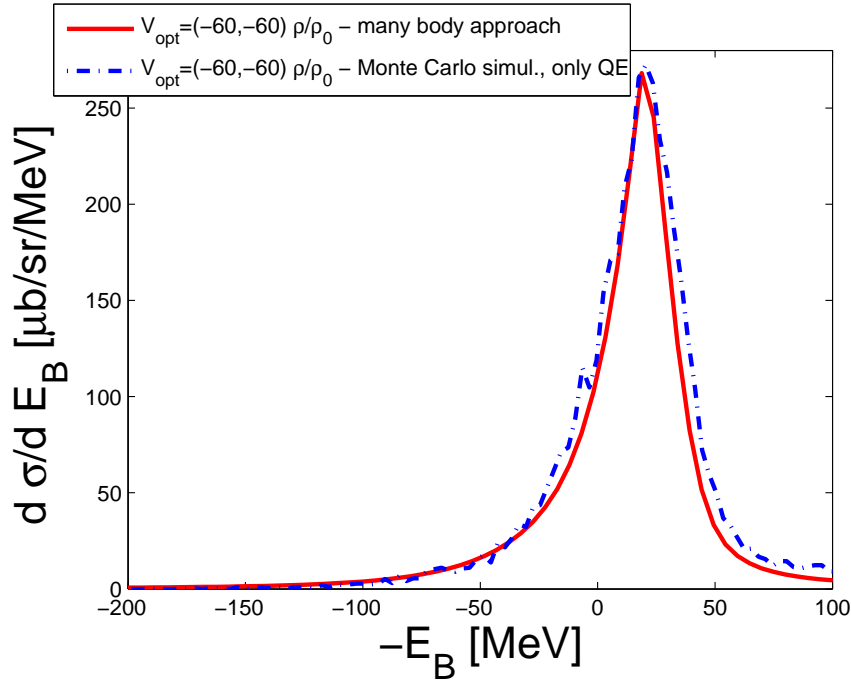


Figure 3: The results of the direct many body evaluation (full line), and of the Monte Carlo simulation considering only the quasi-elastic scattering processes (dashed-dotted line), for  $V_{\text{opt}} = (-60, -60)\rho/\rho_0$  MeV.

Ideally, their corresponding branching ratios should be obtained from relevant microscopic mechanisms, such as the kaon-exchange processes depicted in Fig. 2. There might be, however, other processes such as, for instance, those involving pion exchange. In the present exploratory work, we will consider a much simpler approach consisting of assigning equal probability to each of the above reactions. Noting that the chance of the kaon to find a  $pn$  pair is twice as large as that for  $pp$  or  $nn$  pairs, we finally assign a probability of 3/10 for having a  $p\Sigma$  pair in the final state of  $K^- NN$  absorption, 4/10 for  $n\Sigma$ , 1/10 for  $p\Lambda$  and 2/10 for  $n\Lambda$ .

### 4.3 Nucleon and Hyperon cross-sections

Apart from following the kaons, our calculations also need to consider the quasi-elastic scattering of nucleons,  $\Lambda$  and  $\Sigma$  hyperons on their way through the residual nucleus. The

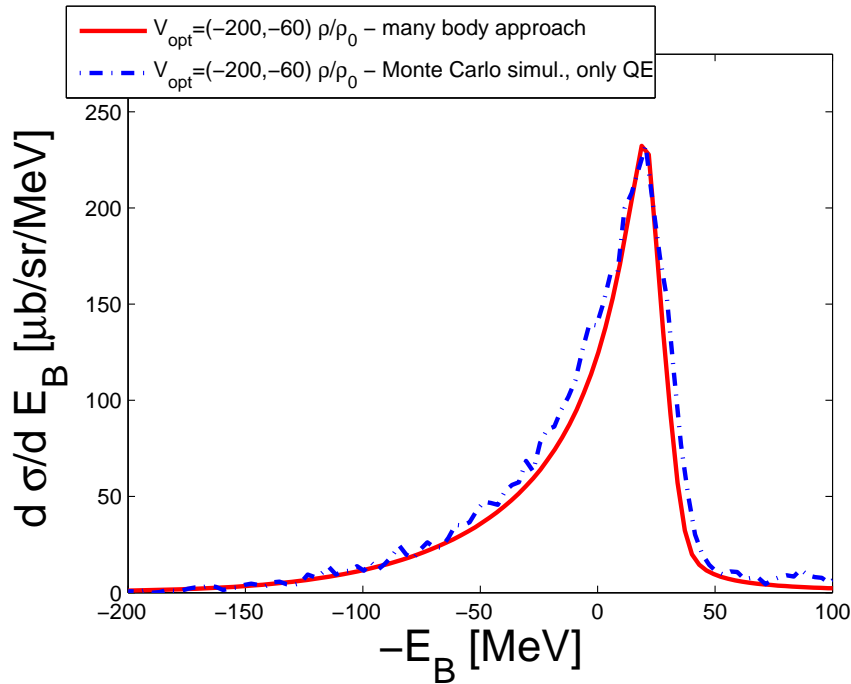


Figure 4: The same as Fig. 3, but for  $V_{\text{opt}} = (-200, -60)\rho/\rho_0$  MeV.

nucleon-nucleon cross sections  $\sigma_{NN}$  for different momenta are taken from the parameterization of Ref. [66], as applied also in other simulations [35, 37]. Given the uncertainties in the hyperon-nucleon cross sections, we may use the relation  $\sigma_{YN} = 2\sigma_{NN}/3$  based on a simple non-strange quark counting rule. This approximation is used for  $\Sigma N$  scatterings. However, other more refined fits to experimental data also exist and, in the case of  $\Lambda N$  scattering, we use the parameterization of Ref. [67], as was also done in Ref. [36].

## 5 Results and discussion

In the first place we would like to compare the results obtained with the diagrammatic many-body method with those of the Monte Carlo simulation when only quasi-elastic scattering is considered. This is shown in Figs. 3, 4 for different optical potentials:  $V_{\text{opt}} = (-60, -60)\rho/\rho_0$  MeV and  $V_{\text{opt}} = (-200, -60)\rho/\rho_0$  MeV correspondingly. As we can see, the two calculations are practically identical in the region of interest. The Monte Carlo simulation produces slightly larger cross sections because it also takes into account the multiple quasi-elastic scattering processes. It is clear that these additional events, which contain a “good” final proton and more than one quasi-elastic collision, are rather rare. However, as we will see, kaon absorption mechanisms produce a substantial amount of energetic nucleons which need to be taken into account.

Before showing the contributions of the new processes, let us first explore the sensitivity of the spectrum to the kaon optical potential. In Figs. 5, 6 we show the results obtained

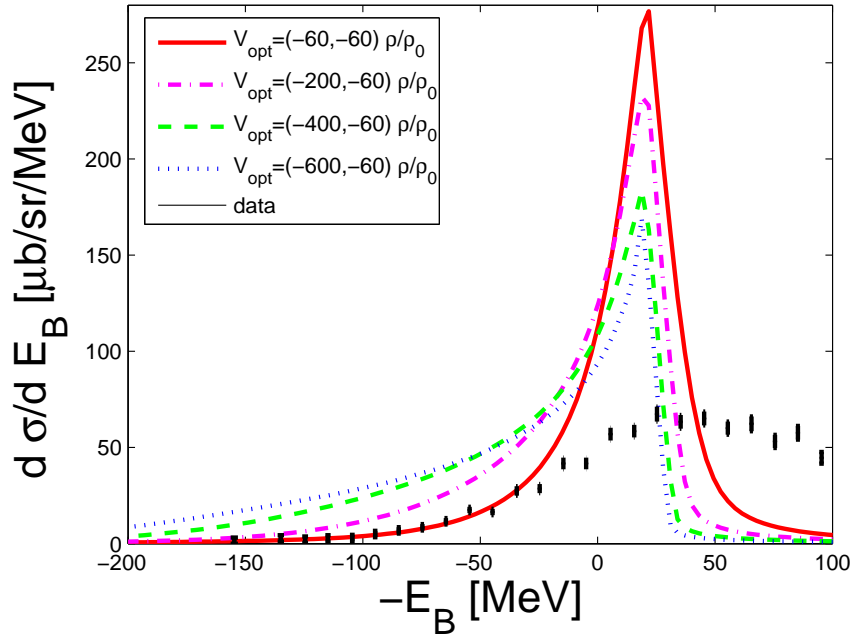


Figure 5: Results obtained using the many body method for kaon potential depths of 60 MeV, 200 MeV, 400 MeV and 600 MeV at normal nuclear density. Experimental data are shown with black bars.

with the many body method employing potential depths of 60 MeV, 200 MeV, 400 MeV and 600 MeV at normal nuclear density. In Fig. 5 we see the absolute distributions plotted together with the experimental spectrum [44]. Increasing the depth of the kaon optical potential produces an enhancement of the cross section in the bound region of kaons, as one might expect intuitively. The height of the theoretical distributions is much larger than that of the experimental cross section. We have tested that our theoretical normalization is correct. Indeed, if we remove the distortion of the incoming kaons and outgoing protons in the many body method, we obtain that the strength of the integrated cross section for the reaction on  $^{12}\text{C}$  is six times the one of the elementary reaction,  $K^-p \rightarrow K^-p$ , at backward angles. The distortion implemented here reduce the nuclear cross section by about a factor 3.5, which is also the same distortion effect obtained in [46].

The different size of the theoretical distribution as compared to the experimental data is in fact showing the removal of events implemented by the coincidence test applied in Ref. [44], demanding that some extra charged particle is detected in a decay counter surrounding the target together with the forward fast proton. It is, however, claimed in [44] that the required coincidence does not change the shape of the spectrum. Assuming this, we can rescale our calculations to give them the size of the experimental distribution, as is illustrated in Fig. 6. The region of main interest corresponds to a deep binding energy for the kaon (i.e. high momenta for the proton) of about 50 MeV or more to the left of the peak, since the quasi-elastic approach ignores many processes populating the spectrum at

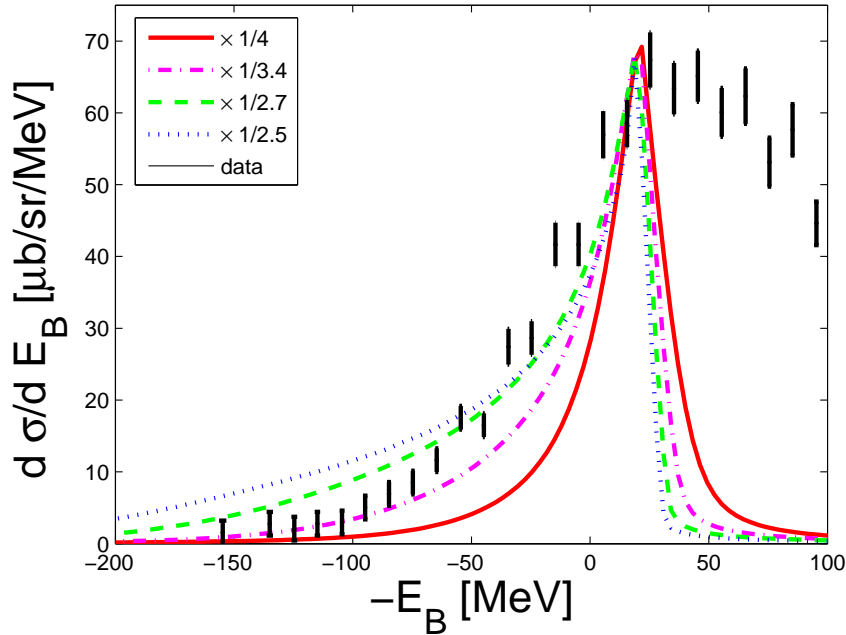


Figure 6: The same results as in Fig. 5, but rescaled to the height of the experimental spectrum [44]. Experimental data are shown with black bars.

low proton momenta. We observe that, to obtain a good description of the spectrum from  $-E_B \sim 0$  down to  $-E_B$  of around  $-100$  MeV one would need optical potential depths as large as 400 MeV, or even 600 MeV, at normal nuclear density, not the 190 MeV claimed in Ref. [44], and even then we observe that the shape is not well reproduced for any of the potentials.

In our opinion, these results indicate the existence of other contributions from processes that are not yet taken into account and/or that the assumption of an energy independent reduction factor due to the coincidence requirement might not be correct. These effects can be investigated within the Monte Carlo simulation developed in this work. In Fig. 7 we show the results of the Monte Carlo simulation obtained with an optical potential  $V_{\text{opt}} = (-60, -60)\rho/\rho_0$  MeV, taking into account only quasi-elastic processes (dash-dotted line) and considering as well one nucleon and two nucleon absorption processes (solid line). We can see that there is a non-negligible amount of strength gained in the region of “bound kaons” due to the new mechanisms. Although not shown separately in the figure, we have seen that one nucleon absorption and multi-scatterings contribute to the region  $-E_B > -50$  MeV. To some extent, this strength can be simulated by the parametric background used in [44]. However, this is not true anymore for the two nucleon absorption processes, which contribute to all values of  $-E_B$ , starting from almost as low as  $-300$  MeV.

It is very important to keep in mind that in the spectrum of [44] the outgoing forward protons were measured in coincidence with at least one charged particle in the decay coun-

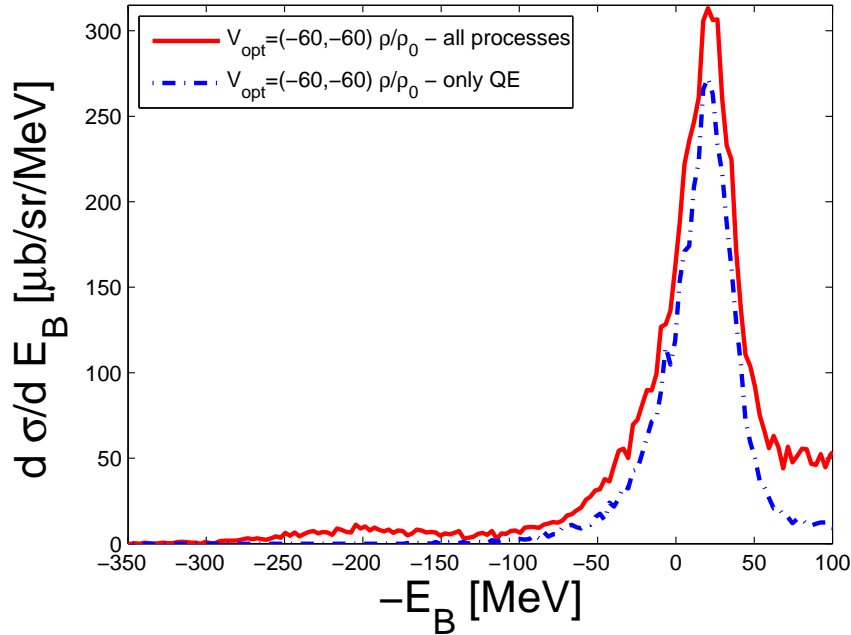


Figure 7: Calculated proton spectra with  $V_{\text{opt}} = (-60, -60)\rho/\rho_0$  MeV, taking into account only quasi-elastic processes (dash-dotted line), and including all processes (solid line).

ters surrounding the target. While a detailed simulation of these experimental conditions is prohibitive we can at least see their consequences by applying the minimal coincidence requirement. As described in Sect. 3.6 we eliminate the events that, for sure, will not produce a coincidence, i.e. those in which, after a primary quasi-elastic collision producing a fast forward proton and a backward kaon, neither particle suffer any further reaction. While it is clear from Fig. 7 that the main source of energetic protons in the  $^{12}\text{C}(K^-, p)$  spectrum is the  $K^-p$  quasi-elastic scattering process, many of these potentially “good” events will be eliminated by the the minimal coincidence requirement. As a result, the shape of the spectrum will change substantially, as clearly illustrated in Fig. 8 upon comparing the bare spectrum obtained with a kaon potential depth of 60 MeV (solid line) with that obtained after the minimal coincidence cut (dashed line). The figure also shows the spectra corresponding to a potential depth of 200 MeV, before (dot-dashed line) and after the coincidence cut (dotted line). We clearly see that the sensitivity of the spectra in the bound region to the optical potential employed is practically lost when the coincidence requirement is applied. These results demonstrate the limited capability of the  $(K^-, p)$  reaction with in-flight kaons to infer the depth of the kaon optical potential. Actually, the bare spectrum would be a more appropriate observable for this task.

To further understand the effects of the coincidence requirement we introduce additional constant suppression factors to the calculated spectrum [68], as seen in Figs. 9 and 10. Figure 9 shows our results using a shallow kaon nucleus optical potential,  $V_{\text{opt}} =$

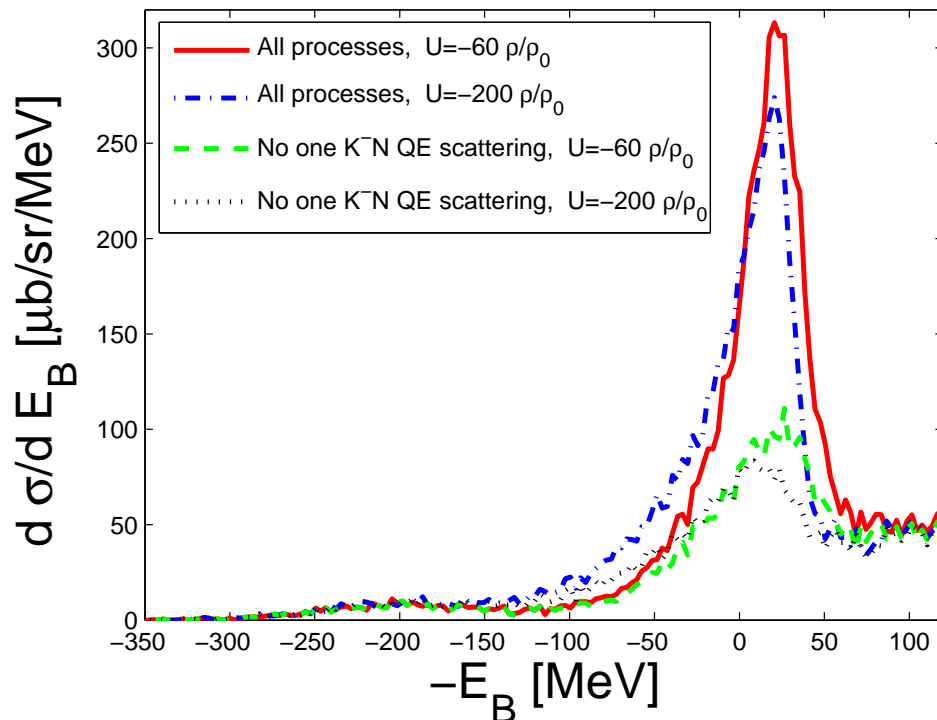


Figure 8: Calculated  $^{12}\text{C}(K^-, p)$  spectra for  $V_{\text{opt}} = (-60, -60)\rho/\rho_0$  MeV and  $V_{\text{opt}} = (-200, -60)\rho/\rho_0$  MeV taking into account all contributing processes (solid and dot-dashed lines), and imposing the minimal coincidence requirement (dashed and dotted lines).

$(-60, -60)\rho/\rho_0$  MeV, as obtained in chiral models. Comparing to experimental data, we can conclude that our results would need a reduction factor of about  $\sim 0.7$ , more or less homogeneous in the “bound” region,  $-E_B < 0$  MeV, while the suppression should be weaker in the continuum, and basically negligible for  $-E_B > 50$  MeV. This picture is natural from the physical point of view, because the spectrum to the right of the peak is populated with lower momentum protons. These are mostly produced in many particle final states, which have a better chance to score the coincidence detectors.

However, if we look at Fig. 10, where the calculations with a deep kaon nucleus optical potential of  $V_{\text{opt}} = (-200, -60)\rho/\rho_0$  MeV are shown, we can conclude that it is much more difficult to obtain an overall description of the data with such a potential, even admitting a strong suppression in the bound region and a negligible one in the continuum.

In spite of the above described behavior, one cannot conclude that the experimental spectrum supports especially one potential depth over the other. However, we want to make clear that, in trying to reproduce the actual data, one necessarily introduces large uncertainties due to the experimental set up. Contrary to what it is assumed in Ref. [44], we have clearly seen in Fig. 8, that the spectrum shape is affected by the required coincidence. In fact, the distortion of the experimental spectrum due to the coincidence requirement can

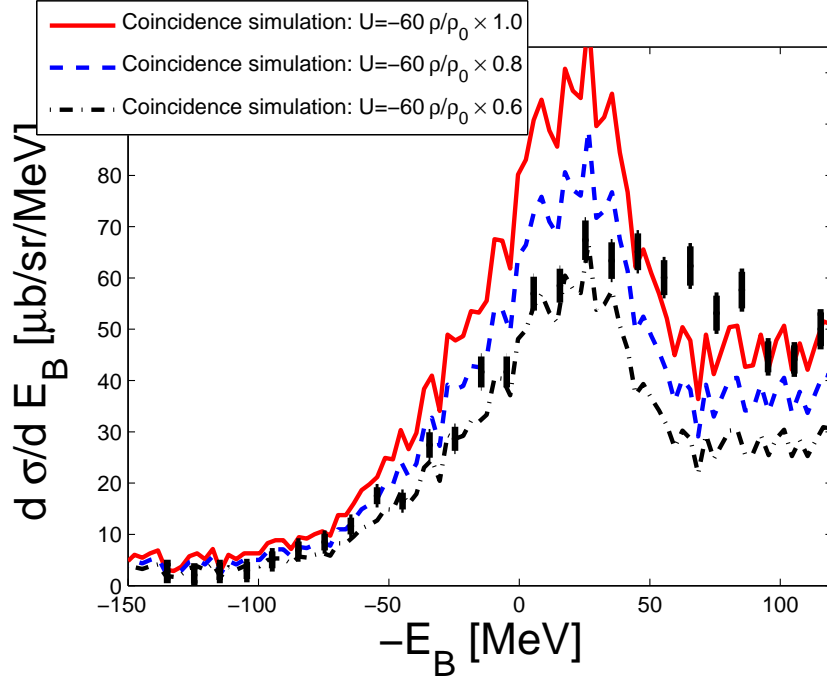


Figure 9: The  $^{12}\text{C}(K^-, p)$  spectrum obtained with  $V_{\text{opt}} = (-60, -60)\rho/\rho_0$  MeV and the minimal coincidence requirement, for several reduction factors. Experimental points are taken from [44].

easily be much bigger than the difference between different potential depths, as seen by the sensitivity of the spectrum to the optical potential displayed in Figs. 5 and 8. Thus, the experiment of Ref. [44] is not appropriate for extracting information on the kaon optical potential. The theoretical analysis of [44] was based on the assumption that the shape of the spectrum does not change with the coincidence requirement. Since we have shown this not to be case, the conclusions obtained there do not hold. Certainly, the experimental data without the coincidence requirement of [44] would be a much more useful observable.

## Acknowledgments

This work is partly supported by the contracts FIS2006-03438, FIS2008-01661 from MICINN (Spain), by CSIC and JSPS under the Spain-Japan research Cooperative program, and by the Generalitat de Catalunya contract 2009SGR-1289. We acknowledge the support of the European Community-Research Infrastructure Integrating Activity “Study of Strongly Interacting Matter” (HadronPhysics2, Grant Agreement n. 227431) under the Seventh Framework Programme of EU. J.Y. is a Yukawa Fellow and this work is partially supported by the Yukawa Memorial Foundation.

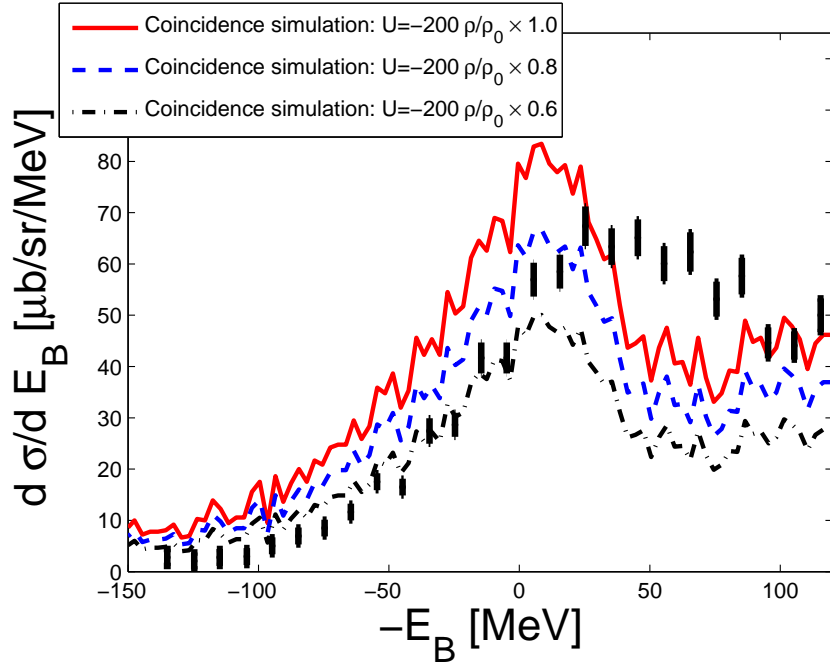


Figure 10: The same as Fig. 9, but for  $V_{\text{opt}} = (-200, -60)\rho/\rho_0$  MeV.

## References

- [1] E. Friedman, A. Gal, and C. J. Batty, Nucl. Phys. A **579**, 518 (1994).
- [2] D. B. Kaplan and A. E. Nelson, Phys. Lett. B **175**, 57 (1986).
- [3] E. Friedman, A. Gal and J. Mares, Phys. Rev. C **60**, 024314 (1999).
- [4] E. Friedman and A. Gal, Phys. Rept. **452**, 89 (2007).
- [5] T. Muto, T. Maruyama and T. Tatsumi, Phys. Rev. C **79**, 035207 (2009).
- [6] T. Maruyama, T. Tatsumi, T. Endo and S. Chiba, Recent Res. Dev. Phys. **7**, 1 (2006).
- [7] T. Maruyama, T. Tatsumi, D. N. Voskresensky, T. Tanigawa, T. Endo and S. Chiba, Phys. Rev. C **73**, 035802 (2006).
- [8] J. Mares, E. Friedman and A. Gal, Phys. Lett. B **606**, 295 (2005).
- [9] J. Mares, E. Friedman and A. Gal, Nucl. Phys. A **770**, 84 (2006).
- [10] D. Gazda, E. Friedman, A. Gal and J. Mares, Phys. Rev. C **76**, 055204 (2007).
- [11] X. H. Zhong, L. Li, C. H. Cai and P. Z. Ning, Commun. Theor. Phys. **41**, 573 (2004).

- [12] X. H. Zhong, G. X. Peng, L. Li and P. Z. Ning, Phys. Rev. C **74**, 034321 (2006).
- [13] L. Dang, L. Li, X. H. Zhong and P. Z. Ning, Phys. Rev. C **75**, 068201 (2007).
- [14] M. Lutz, Phys. Lett. B **426**, 12 (1998).
- [15] A. Ramos and E. Oset, Nucl. Phys. A **671**, 481 (2000).
- [16] J. Schaffner-Bielich, V. Koch and M. Effenberger, Nucl. Phys. A **669**, 153 (2000).
- [17] A. Cieply, E. Friedman, A. Gal and J. Mares, Nucl. Phys. A **696**, 173 (2001).
- [18] L. Tolos, A. Ramos and E. Oset, Phys. Rev. C **74**, 015203 (2006).
- [19] S. Hirenzaki, Y. Okumura, H. Toki, E. Oset and A. Ramos, Phys. Rev. C **61**, 055205 (2000).
- [20] A. Baca, C. Garcia-Recio and J. Nieves, Nucl. Phys. A **673**, 335 (2000).
- [21] Y. Akaishi and T. Yamazaki, Phys. Rev. C **65**, 044005 (2002).
- [22] Y. Akaishi, A. Dote and T. Yamazaki, Phys. Lett. B **613**, 140 (2005).
- [23] E. Oset and H. Toki, Phys. Rev. C **74**, 015207 (2006).
- [24] T. Hyodo and W. Weise, Phys. Rev. C **77**, 035204 (2008).
- [25] T. Yamazaki and Y. Akaishi, Nucl. Phys. A **792**, 229 (2007).
- [26] E. Oset, V. K. Magas, A. Ramos and H. Toki, proceedings of the IX International Conference on Hypernuclear and Strange Particle Physics, Mainz (Germany), October 10-14, 2006. Edited by J. Pochodzalla and Th. Walcher, (Springer, Germany, 2007), 263.
- [27] A. Ramos, V. K. Magas, E. Oset and H. Toki, Nucl. Phys. A **804**, 219 (2008).
- [28] N. V. Shevchenko, A. Gal, J. Mares and J. Revai, Phys. Rev. C **76**, 044004 (2007).
- [29] A. Dote, T. Hyodo and W. Weise, Nucl. Phys. A **804**, 197 (2008).
- [30] Y. Ikeda and T. Sato, Phys. Rev. C **76**, 035203 (2007).
- [31] T. Yamazaki and Y. Akaishi, Phys. Rev. C **76**, 045201 (2007).
- [32] T. Suzuki *et al.*, Phys. Lett. B **597**, 263 (2004).
- [33] M. Agnello *et al.* [FINUDA Collaboration], Phys. Rev. Lett. **94**, 212303 (2005).
- [34] M. Agnello *et al.* [FINUDA Collaboration], Phys. Lett. B **654**, 80 (2007).

- [35] V. K. Magas, E. Oset, A. Ramos and H. Toki, Phys. Rev. C **74**, 025206 (2006); A. Ramos, V. K. Magas, E. Oset and H. Toki, Eur. Phys. J. **A31**, 684 (2007).
- [36] V. K. Magas, E. Oset, A. Ramos and H. Toki, [arXiv:nucl-th/0611098].
- [37] V. K. Magas, E. Oset and A. Ramos, Phys. Rev. C **77**, 065210 (2008); [arXiv:0901.1086 [nucl-th]]; [arXiv:0901.3306 [nucl-th]].
- [38] T. Suzuki *et al.* [KEK-PS E549 Collaboration], Phys. Rev. C **76**, 068202 (2007).
- [39] M. Sato *et al.*, Phys. Lett. B **659**, 107 (2008).
- [40] M. Agnello *et al.* [FINUDA Collaboration], and C-12 Nucl. Phys. A **775**, 35 (2006).
- [41] S. Piano, talk at the 10th International Conference on Hypernuclear and Strange Particle Physics (Hyp X), "RICOTTI" in Tokai, Ibaraki, Japan, September 14-18, 2009.
- [42] G. Bendiscioli *et al.*, Nucl. Phys. **A789**, 222 (2007).
- [43] T. Yamazaki *et al.*, arXiv:0810.5182 [nucl-ex].
- [44] T. Kishimoto *et al.*, Prog. Theor. Phys. **118**, 181 (2007).
- [45] O. Morimatsu and K. Yazaki, Prog. Part. Nucl. Phys. **33**, 679 (1994).
- [46] J. Yamagata, H. Nagahiro and S. Hirenzaki, Phys. Rev. C **74**, 014604 (2006).
- [47] J. Yamagata, H. Nagahiro, R. Kimura and S. Hirenzaki, Phys. Rev. C **76**, 045204 (2007).
- [48] J. Yamagata-Sekihara, D. Jido, H. Nagahiro and S. Hirenzaki, Phys. Rev. C **80**, 045204 (2009).
- [49] J. Yamagata and S. Hirenzaki, Eur. Phys. J. **A31**, 255 (2007).
- [50] W. M. Alberico, A. Molinari, T. W. Donnelly, E. L. Kronenberg and J. W. Van Orden, Phys. Rev. C **38**, 1801 (1988).
- [51] A. Gil, J. Nieves and E. Oset, Nucl. Phys. A **627**, 543 (1997).
- [52] R. C. Carrasco, E. Oset and L. L. Salcedo, Nucl. Phys. A **541**, 585 (1992).
- [53] E. Oset, D. Strottman, H. Toki and J. Navarro, Phys. Rev. C **48**, 2395 (1993).
- [54] M. Urban and J. Wambach, Phys. Rev. C **65**, 067302 (2002).
- [55] C. W. De Jager, H. De Vries and C. De Vries, Atom. Data Nucl. Data Tabl. **14**, 479 (1974).

- [56] E. Friedman, A. Gal and J. Mares, Nucl. Phys. A **761**, 283 (2005)
- [57] B. Conforto et al., Nucl. Phys. **B105**, 189 (1976).
- [58] L. L. Salcedo, E. Oset, M. J. Vicente-Vacas and C. Garcia-Recio, Nucl. Phys. A **484**, 557 (1988).
- [59] R. C. Carrasco, M. J. Vicente Vacas and E. Oset, Nucl. Phys. A **570**, 701 (1994).
- [60] A. Gil, J. Nieves and E. Oset, Nucl. Phys. A **627**, 599 (1997).
- [61] A. Ramos, M. J. Vicente-Vacas and E. Oset, Phys. Rev. C **55**, 735 (1997) [Erratum-  
ibid. C **66**, 039903 (2002)].
- [62] G. Garbarino, A. Parreno and A. Ramos, Phys. Rev. Lett. **91**, 112501 (2003).
- [63] T. Kishimoto, private communication.
- [64] C. Amsler *et al.* [Particle Data Group], Phys. Lett. B **667**, 1 (2008);  
<http://pdg.lbl.gov/>
- [65] P. A. Katz, K. Bunnell, M. Derrick, T. Fields, L. G. Hyman and G. Keyes, Phys. Rev. D **1**, 1267 (1970).
- [66] J. Cugnon, D. L'Hôte and J. Vandermeulen, Nucl. Instrum. Meth. **B111**, 215 (1996).
- [67] S. K. Singh and M. J. Vicente Vacas, Phys. Rev. **D74**, 053009 (2006).
- [68] V.K. Magas, J. Yamagata-Sekihara, S. Hirenzaki, E. Oset, A. Ramos, [arXiv:0911.2091 [nucl-th]]; A. Ramos, V.K. Magas, J. Yamagata-Sekihara, S. Hirenzaki, E. Oset, [arXiv:0911.4841 [nucl-th]]; E. Oset, et al., [arXiv:0912.3145 [nucl-th]].